

# Probabilistic Simulation for Nanocomposite Fracture

Christos C. Chamis

*NASA Glenn Research Center, Cleveland, Ohio 44135*

## Abstract

A unique probabilistic theory is described to predict the uniaxial strengths and fracture properties of nanocomposites. The simulation is based on composite micromechanics with progressive substructuring down to a nanoscale slice of a nanofiber where all the governing equations are formulated. These equations have been programmed in a computer code. That computer code is used to simulate uniaxial strengths and fracture of a nanofiber laminate. The results are presented graphically and discussed with respect to their practical significance. These results show smooth distributions from low probability to high.

## 1.0 Introduction

The research in the nanoscale technology has exploded over the recent past. An indication of this explosion is that the Society of Aerospace Material and Processing Engineers (SAMPE) Conference is devoting four sessions of about six papers each in the last 5 years. These papers cover practically all current research activities. The majority of the research is devoted to processing because of the difficulties involved in making a useful material [1]. A few investigators have been fortunate to make some testing samples, which they subsequently tested to obtain limited data [2]. A few other investigators researched the characterization of fatigue [3] and creep [4]. A couple of papers explored the construction of nanocomposites for rocket ablative material [5] and for carbon nanotubes for adaptive structures [6]. One paper ventured to describe a computer simulation of macroscopic properties of carbon nanotubes polymer composites [7]. However, there are no results of what special macroscopic properties are included. Reference [7] shows one stress strain curve and citation of several references. One recent article [8] describes multiscale modeling and simulation of nanostructural materials from atomistic to micromechanics. This article does not include information on nanocomposites, but it mentions that mechanistic models will be needed in the end. It is becoming abundantly clear that no holistic approach has been used to investigate the mechanistic prediction of uniaxial strength and fracture.

In this paper a unique mechanistic method is described to probabilistically simulate five uniaxial strengths and fracture of a nanofiber uniaxial composite. The mechanistic deterministic simulation of all uniaxial properties is described in a previous paper [9].

## 2.0 Fundamentals

The fiber alignment with uniform dispersion is not met in nanocomposites. It is assumed herein that the fibers are aligned only for predicting “point” through-the-

thickness properties. The fustiness can be simulated by estimating the angle of single fibers through the thickness. Therefore, it is assumed that an aligned unidirectional typical section of a nanocomposite is as illustrated schematically in Fig. 1 on the left 1(a). A nanoply is schematically shown in Fig. 1 on the right 1(b). The input includes the constituent material properties, tables 1 and 2, the fabrication parameters, environmental, and the loading conditions.

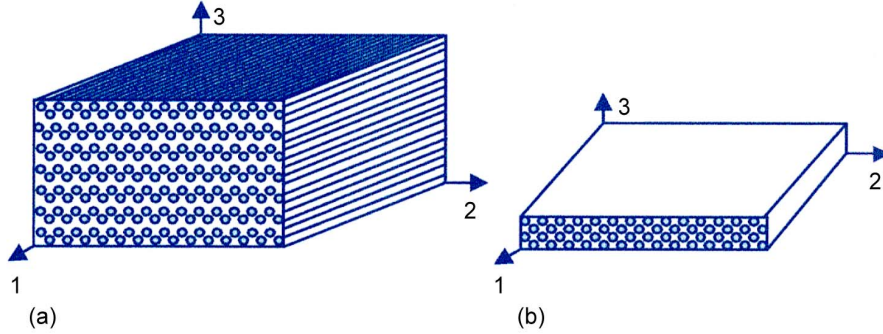


Fig. 1. Unidirectional nanocomposite typical section. (a) Nanocomposite. (b) Nanoply.

Table 1. T300 Graphite Nanofiber (Pyrograf II) Properties

[Conversion factors: 110 nm =  $2.756 \times 10^{-6}$  in.; psi = 6.89 Pa; lb/in.<sup>3</sup> = 1146 kg/cm<sup>3</sup>; in./in./°F = (2/5); cm/cm/°F; Btu = 1055 joules.]

Description	Symbol	Value	Units
Number of fibers per end	Nf	1.0	number
Filament equivalent diameter	df	$2.756 \times 10^{-6}$	in.
Weight density	Rhof	0.064	lb/in.**3
Normal moduli (11)	Ef11	$1.0 \times 10^9$	psi
Normal moduli (22)	Ef22	$7.0 \times 10^7$	psi
Poisson's ratio (12)	Nuf12	0.2	Nondimensional
Poisson's ratio (23)	Nuf23	0.25	Nondimensional
Shear moduli (12)	Gf12	$5.0 \times 10^7$	psi
Shear moduli (23)	Gf23	$3.5 \times 10^7$	psi
Thermal expansion coefficient (11)	Alfaf11	$-5.5 \times 10^{-7}$	in./in./°F
Thermal expansion coefficient (22)	Alfaf22	$5.6 \times 10^{-6}$	in./in./°F
Heat conductivity (11)	Kf11	444.0	Btu/hr/ft <sup>2</sup> /°F/in.
Heat conductivity (22)	Kf22	4.0	Btu/hr/ft <sup>2</sup> /°F/in.
Heat capacity	Cf	0.22	Btu/lb/°F
Dielectric strength (11)	KeF11	0.0	V/in.
Dielectric strength (22)	Kef22	0.0	V/in.
Dielectric constant (11)	Gamma11	0.0	in./V
Dielectric constant (22)	Gamma22	0.0	in./V
Capacitance	Cef	0.0	V
Resistivity	Ref	0.0	Ω-in.
Tensile strength	SfT	$8.0 \times 10^5$	psi
Compressive strength	SiC	$6.0 \times 10^5$	psi
Shear strength	SfS	$4.0 \times 10^5$	psi
Normal damping capacity (11)	psi11f	0.38	%Energy
Normal damping capacity (22)	psi22f	6.3	%Energy
Shear damping capacity (12)	psi12f	3.34	%Energy
Shear damping capacity (23)	psi23f	6.3	%Energy
Melting temperature	TMf	6000.0	°F

Table 2. Intermediate Modulus High-Strength Matrix (Epoxy)

[Conversion factors: 110 nm =  $2.756 \times 10^{-6}$  in.; psi = 6.89 Pa; lb/in<sup>3</sup> = 1146 kg/cm<sup>3</sup>; in./in./°F = (2/5); cm/cm/°C; Btu = 1055 joules]

Description	Symbol	Value	Units
Weight density	Rhom	0.044	lb/in.**3
Normal modulus	Em	500000.0	psi
Poisson's ratio	Num	0.35	Nondimensional
Thermal expansion coefficient	Alfa m	$3.6 \times 10^{-5}$	in./in./°F
Heat conductivity	Km	0.008681	Btu/hr/ft <sup>2</sup> /°F/in.
Heat capacity	Cm	0.25	Btu/lb/°F
Dielectric strength	Kem	0.0	V/in.
Dielectric constant	Gammam	0.0	in./V
Capacitance	Cem	0.0	V
Resistivity	Rem	0.0	Ω-in.
Moisture expansion coefficient	Betam	0.0033	in./in./%moisture
Diffusivity	Dm	$2.16 \times 10^{-7}$	in.**2/hr
Saturation	Mm	0.0	%moisture
Tensile strength	SmT	15000.0	psi
Compressive strength	SmC	35000.0	psi
Shear strength	SmS	13000.0	psi
Allowable tensile strain	eps mT	0.02	in./in.
Allowable compression strain	eps mC	0.05	in./in.
Allowable shear strain	eps mS	0.035	in./in.
Allowable torsional strain	eps mTOR	0.035	in./in.
Normal damping capacity	psiNM	6.6	%energy
Shear damping capacity	psiSm	6.9	%energy
Void heat conductivity	Kv	0.0012	Btu/hr/in./°F
Glass transition temperature	Tgdr	420.0	°F
Melting temperature	TMm	0.0	°F

The strength prediction is expedited by the following geometric diagrams: An exploded view of nanoscale isolation of a typical part is shown in Fig. 2 with nanoscale dimensions. A single nanofiber schematic with substructuring is shown in Fig. 3(a), and a typical subslice is shown in Fig. 3(b).

A nanosubply with its corresponding stresses is shown in Fig. 4. The nanomechanics predictive equations are derived by using Fig. 4. The equations used are all programmed in ICAN/JAVA [10].

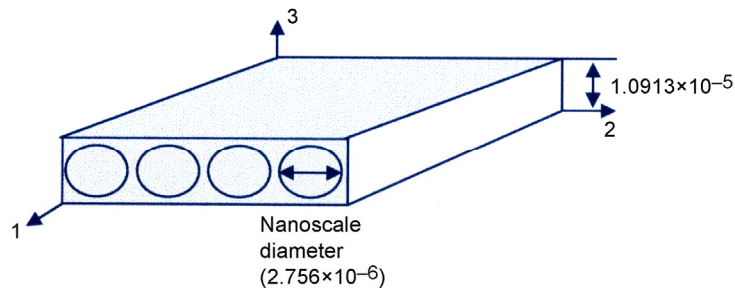


Fig. 2. Nanoscale isolation of a typical part (units are in in.).

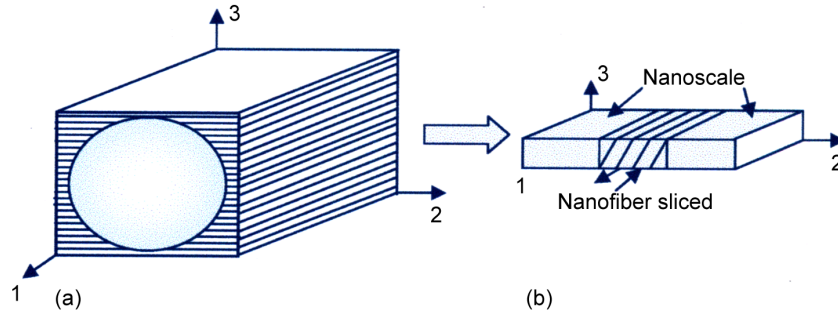


Fig. 3. Nanofiber substructuring. (a) Several slices through the thickness. (b) Nanofiber sliced.

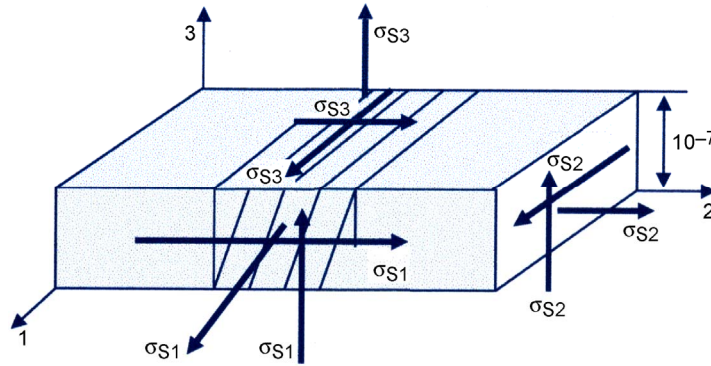


Fig. 4. Nanostresses on a nanosubply (units are in in.).

Prior to describing the results obtained, it is instructive to describe the interphase and how it is modeled. The schematics in Fig. 5 show a vertical section, upper figure part, with unit thickness of the nanocomposite and a single fiber in it. As can be seen in the slice, lower figure, the fiber interphase is represented by a series of progressively larger volume voids starting with the smallest near the matrix interface and ending with the largest in the fiber interface. It can be visualized that the stress in the matrix will be magnified because of the voids. This magnification is shown in Fig. 6 for a specific nanocomposite with 0.05 fiber volume ratio and with void volume ratio varying from 0.05 to 0.4. The interesting point to note in the lower part of Fig. 5 is that the matrix is continuous even though it is filled with progressively larger voids; otherwise the stresses will not be continuous in the matrix. It is instructive to elaborate a bit further with the geometry of Fig. 5, lower part. In order to fill up a conventional ply of 0.005 in. thick and a width of 1 in., it will require about  $1 \times 10^6$  nanofibers, a very large number indeed. The magnification factor of the voids effect in the interphase is shown in Fig. 6. As can be seen in Fig. 6, the magnification factor increases from a value of about 1.1 to a maximum of about 2. Therefore, the maximum void effect will be nearest to the fiber interface.

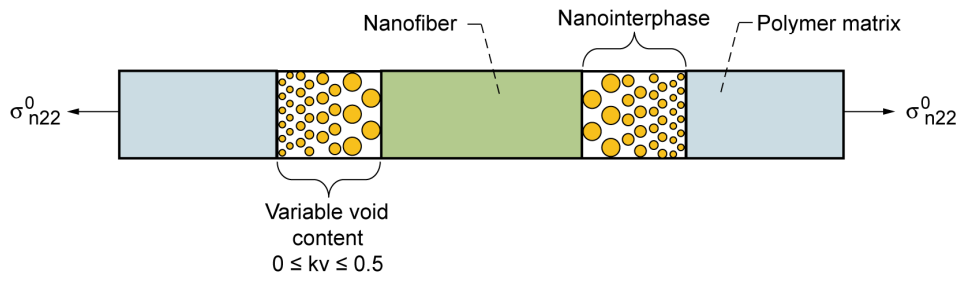
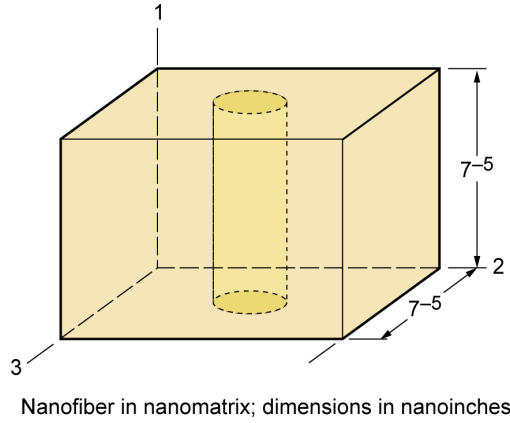


Fig. 5. Vertical section a composite nanocell through nanofiber center.

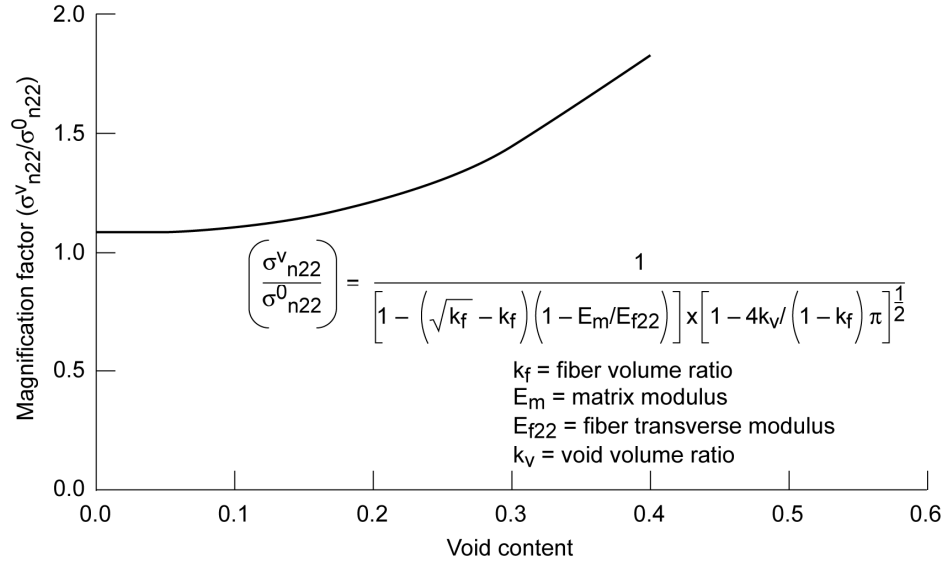


Fig. 6. Nanocomposite magnification factor.

### 3.0 Results and Discussion

In this section the probabilistic results are presented and discussed starting with the large voids in the interphase. The probabilistic void magnification factor is shown graphically in Fig. 7. It can be seen in Fig. 7 that the larger the void content the greater the deviation. The left most figure is closest to the matrix

interphase fiber interface while the right most curve is closest to the interphase interface. The respective scatter is about 0.1 for the curve closest to the matrix to about 1 for the curve closest to the fiber. The corresponding sensitivities are shown in Fig. 8. It can be seen in this figure that the void sensitivities on the magnification factor is large. The probabilistic void effects on the uniaxial strengths are plotted in Fig. 9. Figure 9(a) shows the spread in the longitudinal tensile strength; Fig. 9(b), in the longitudinal compressive strength; Fig. 9(c), in the transverse tensile strength and Fig. 9(d) in the transverse compressive strength. It can be seen in Fig. 9 that the distribution for the two longitudinal strengths is relatively large. It is from 150 to 650 ksi, for tensile strength and with a distribution of about 500 ksi, and for the compressive strength is from 140 to 500 ksi or a distribution of about 360 ksi. The corresponding probabilistic sensitivities are plotted in Fig. 10 for tensile and Fig. 11 for compressive. It can be seen in these two figures that there is no difference in the sensitivities for the three probabilities. The probabilistic intralaminar shear strength is plotted in Fig. 12. The distribution in this strength is from about 6,000 to ~16,000 psi or ~10 ksi spread. It is a relatively wide distribution from lowest probability to the highest. The corresponding probability sensitivities are plotted in Fig. 13 for uniaxial nano transverse tensile strength. Note that these probabilistics are for 0.0001, 0.50, and 0.9999. They are about the same and may be easily interchangeable as well as for three fiber volume ratios.

The respective sensitivities for the other nanouniaxial strengths are the same and are not shown. The fracture for uniaxial nanofiber composites are the same as their respective uniaxial nanofiber uniaxial strengths.

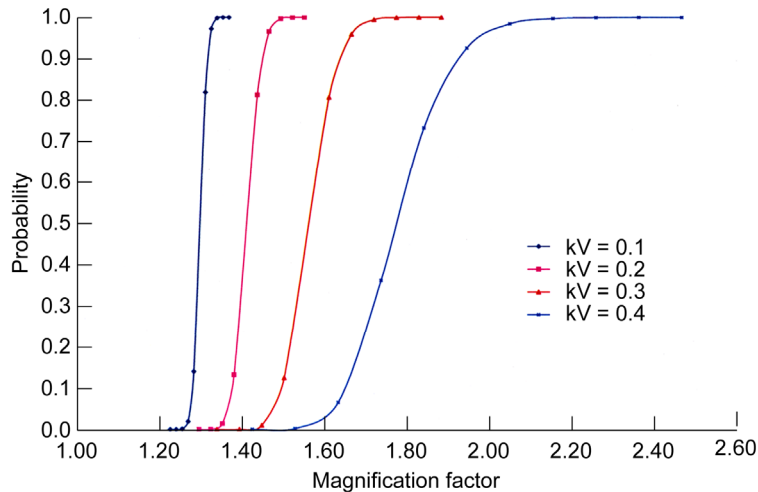


Fig. 7. Probabilistic magnification factor of voids in the interphase.

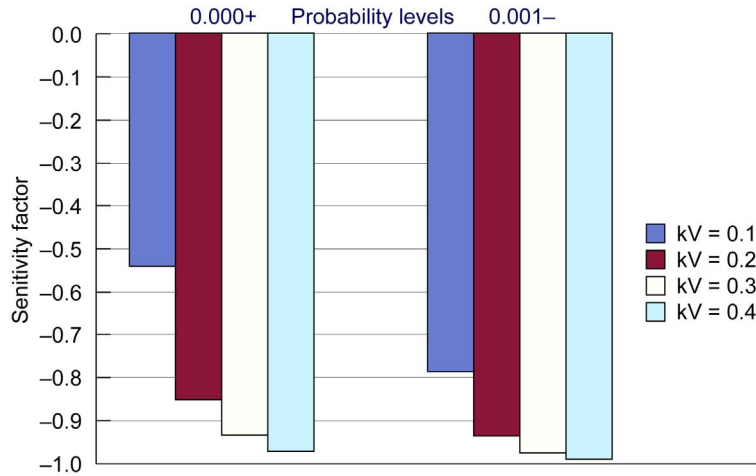


Fig. 8. Voids sensitivities on the interphase magnification factor.

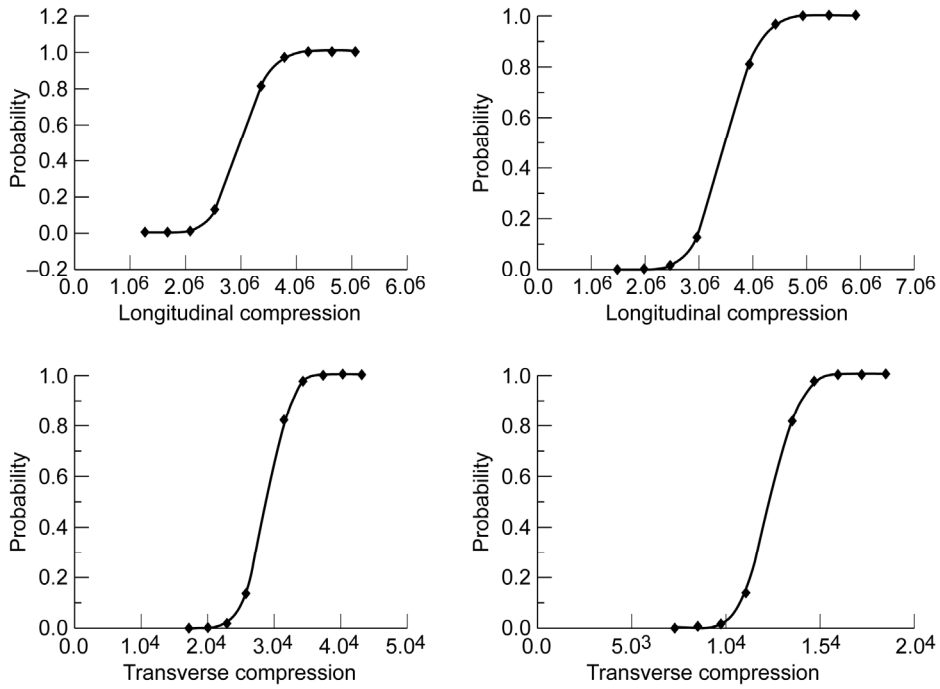


Fig. 9. Probabilistically plotted nanouniaxial strengths.

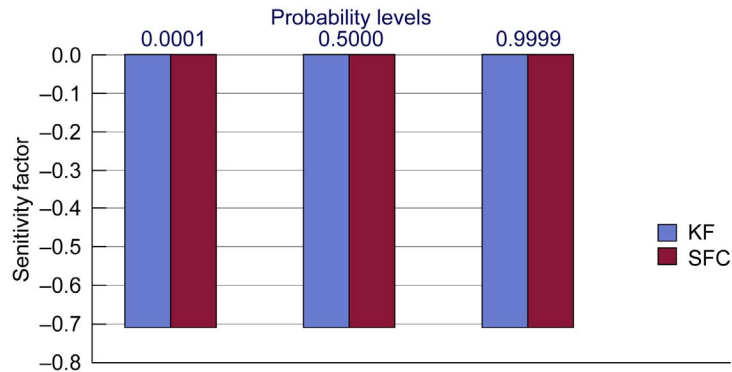


Fig. 10. Probabilistic sensitivities for nano longitudinal uniaxial strength.

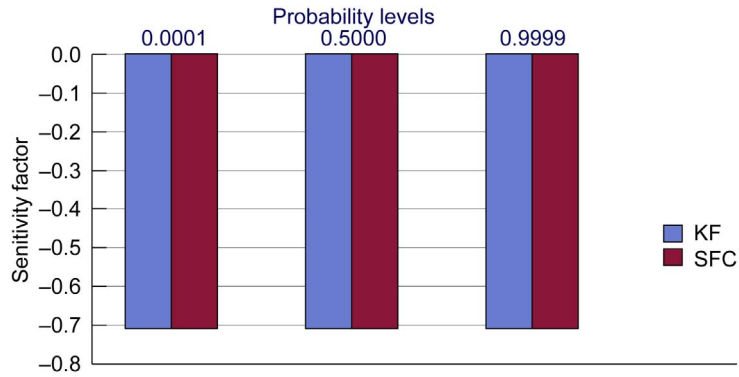


Fig. 11. Probabilistic sensitivities for the nanocompressive uniaxial strength.

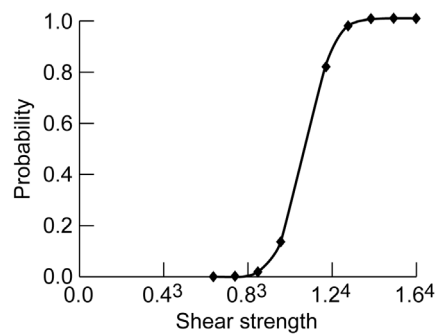


Fig. 12. Probabilistically plotted intralaminar uniaxial shear strength.

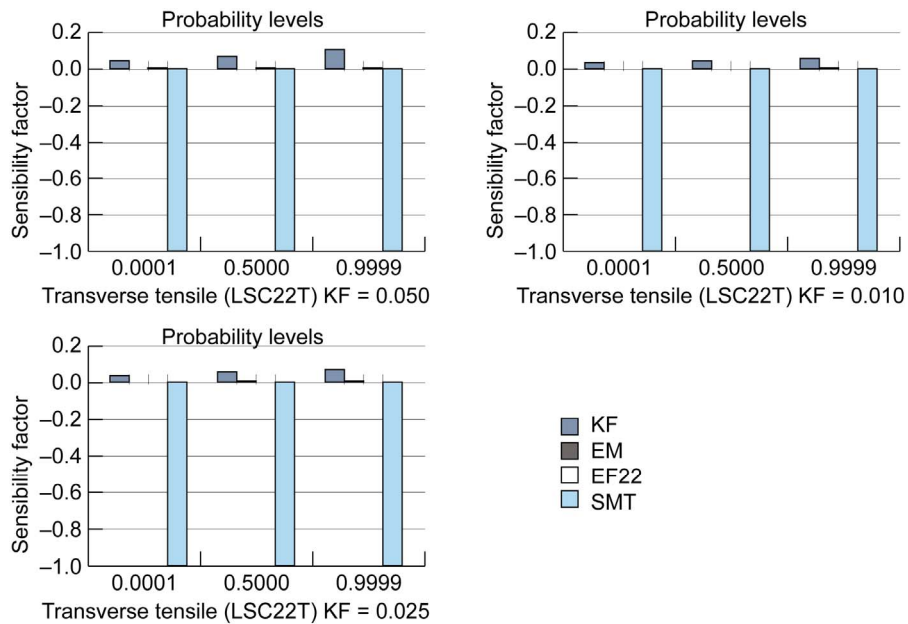


Fig. 13. Probabilistic sensitivities for nanouniaxial transverse tensile strength for three different probabilities.

#### **4.0 Concluding Remarks**

The salient remarks from an investigation to characterize an aligned monofiber nanolaminate are as follows:

1. The characterization for the nanolaminate (composite) was based on a series of progressive substructuring down a sliced single-diameter fiber.
2. The theoretical development and all the equations are included in a computer code called ICAN/JAVA.
3. The uniaxial strength and fracture includes two fabrication parameters, 5-nano-uniaxial strengths/fracture.
4. The nanolaminate investigated consists of single nanofiber laminate with 0.05 fiber volume ratio.
5. The effects of the interphase are especially important and are represented by progressively large amounts of voids from the matrix interface to the fiber interphase.
6. The probabilistic evaluation characterizes the effects of uncertainties in all participating variables.
7. The voids uncertainties indicate as the void volume ratio increases the distribution increases as well.
8. The voids contribute significantly to matrix dominated strengths/fracture.

## References

- [1]. M. Jose, J. Tyner, E. Nyairo, D. Dean, Synthesis and processing of aligned carbon nanotube based fibers, 49th Int SAMPE Symp and Exhib Conf Proc, 2004.
- [2] G. Ayalasonmayajuala, A. Garg, S. Kapila, K. Chandrashekhara, V. Flanigan, Fabrication and evaluation of rice hull derived nano silica composites, SAMPE, 49th Int Symp and Exhib Conf Proc, 2004.
- [3] T. Karaki, J.P. Killgore, J.C. Seferis, Characterization of fatigue behavior of polynanomeric matrix composites, SAMPE, 49th Int Symp and Exhib Conf Proc, 2004.
- [4] A. Ranade, N.A. D'Souza, K. Nayak, B. Gnade, D. Fairbrother, Correlation between creep-recovery, crystallization and dispersion of linear low density polyethylene nanocomposite films, SAMPE, 48th Int Symp and Exhib Conf Proc, 48, 1, 2164–2176, 2003.
- [5] J.H. Koo, H. Stretz, J. Weispfenning, Z.P. Luo, W. Wootan, Nanocomposite rocket ablative materials: Subscale ablation test, 49th Int SAMPE Symp and Exhib Conf Proc, 2004.
- [6] S. Muhle, H.P. Monner, P. Wiersch, P., Carbon-nanotubes for adaptive structures, SAMPE, 48th Int Symp and Exhib, 48, 1, 1181–1190, 2003.
- [7] D. Srivastava, C. Wei, Computer simulations of macroscopic properties of carbon-nanotube polymer composites, SAMPE, 48th Int Symp and Exhib, 48, 1, 2153–2163, 2003.
- [8] T.S. Gates et al., Computational materials: Multi-scale modeling and simulation of nanostructural materials. *Comp Sci T*, 65 (2005), 2416–2434.
- [9] C.C. Chamis, Composite nanomechanics properties prediction, NASA/TM—2007-214673.
- [10] L.M. Handler, C.C. Chamis, ICAN/JAVA computer code.